International Journal of Nanomedicine

Dovepress
open access to scientific and medical research

Open Access Full Text Article

ORIGINAL RESEARCH

Spherulitic copper–copper oxide nanostructure-based highly sensitive nonenzymatic glucose sensor

This article was published in the following Dove Press journal:
International Journal of Nanomedicine
27 August 2015
Number of times this article has been viewed

Gautam Das
Thao Quynh Ngan Tran
Hyon Hee Yoon

Department of Chemical and Biological Engineering, Gachon University, Seongnam, Republic of South Korea

Abstract: In this work, three different spherulitic nanostructures Cu–CuO_A, Cu–CuO_B, and Cu–CuO_C were synthesized in water-in-oil microemulsions by varying the surfactant concentration (30 mM, 40 mM, and 50 mM, respectively). The structural and morphological characteristics of the Cu–CuO nanostructures were investigated by ultraviolet–visible (UV–vis) spectroscopy, X-ray diffraction, scanning electron microscopy, and high-resolution transmission electron microscopy techniques. The synthesized nanostructures were deposited on multiwalled carbon nanotube (MWCNT)-modified indium tin oxide (ITO) electrodes to fabricate a nonenzymatic highly sensitive amperometric glucose sensor. The performance of the ITO/MWCNT/Cu–CuO electrodes in the glucose assay was examined by cyclic voltammetry and chronoamperometric studies. The sensitivity of the sensor varied with the spherulite type; Cu–CuO_A, Cu–CuO_B, and Cu–CuO_C exhibited a sensitivity of 1,229, 3,012, and 3,642 μA $mM^{-1}\cdot cm^{-2}$, respectively. Moreover, the linear range is dependent on the structure types: 0.023–0.29 mM, 0.07–0.8 mM, and 0.023–0.34 mM for Cu–CuO_A, Cu–CuO_B, and Cu–CuO_C, respectively. An excellent response time of 3 seconds and a low detection limit of 2 μM were observed for Cu–CuO_B at an applied potential of +0.34 V. In addition, this electrode was found to be resistant to interference by common interfering agents such as urea, cystamine, L-ascorbic acid, and creatinine. The high performance of the Cu–CuO spherulites with nanowire-to-nanorod outgrowths was primarily due to the high surface area and stability, and good three-dimensional structure. Furthermore, the ITO/MWCNT/Cu–CuO_B electrode applied to real urine and serum sample showed satisfactory performance.

Keywords: copper oxide, multiwalled carbon nanotubes, glucose sensor, cyclic voltammetry

Introduction

The scope of nanomaterials with controlled shape, size, and selectivity is very appealing considering that their physicochemical properties vary accordingly.[1] Thus, controlling the morphological hierarchy is important for tuning nanomaterial properties.[2] Compared with other transition metal oxides, copper oxide nanostructures have been an attractive choice for wide range of applications such as in antimicrobials,[3,4] chemical and biological sensors,[5,6] optoelectronics,[7] photonics, and electronic devices[8] owing to their advantageous properties such as high surface area, high conducting properties, and relatively low prices.[3] Copper oxide with controlled shape and size at the nanoscopic level may influence the catalytic, optical, and electrical properties, limiting the use of these nanomaterials and reducing the costs.[9] These nanostructures have a low band gap (1.2–1.6 eV) with high catalytic activity and reasonable stability.[10] Various methodologies have been employed to synthesize copper oxide-based nanostructures with

Correspondence: Hyon Hee Yoon
Department of Chemical and Biological Engineering, Saerom Kwan, 1342 Seongnam Daero, Sujeong Gu, Seongnam Si, Gyeonggi Do, Republic of Korea, 461–701
Tel +82 31 750 8518
Fax +82 31 750 5363
Email hhyoon@gachon.ac.kr

submit your manuscript | www.dovepress.com
Dovepress
http://dx.doi.org/10.2147/IJN.S88317

controlled morphologies.[9,11] Jiang et al prepared different nanostructures of CuO by hydrothermal treatment of copper acetate in alkaline pH.[12] Zhang et al[13] reported the synthesis of nanoribbon-like mesoporous copper oxide by a soft template approach by employing tetraoctylammonium bromide. Copper oxide with urchin-like morphology was obtained by Keyson et al[14] by microwave irradiation of basic copper carbonated ($CuCO_3 \cdot Cu(OH)_2$) in poly(ethylene glycol). These repetitive self-generated superstructures are attractive because of their diverse structural attributes, advantageous large surface-to-volume ratios, and promising complex functions.[9] Thus, the synthesis of nanostructures via the assembly of nanoscale building blocks can create different architectures with controlled morphology.

A well-dispersed water-in-oil emulsion proved to serve as a dynamic and robust microreactor to obtain nanostructures with a well-defined architecture.[15] These reverse micelles are formed by the self-organization of the surfactant such as cetyltrimethyl ammonium bromide (CTAB) in a nonpolar solvent so that the hydrophilic part forms the core and the hydrophobic part forms the shell.[16] Ranjan et al obtained copper monooxalate monohydrate nanoparticles by using a reverse micellization process.[17] Cu and Pd core–shell bimetallic nanostructures were synthesized by Zhou et al.[18] CuO[19] and Cu_2O[20] nanoparticles have also been studied in water-in-oil microemulsions. The soft template-based synthetic technique generates structures with well-defined features and better size control beneficial for the fabrication of high-performance microscale devices.[21]

Diabetes is a chronic disease that affects millions of people worldwide.[9] Frequent testing of physiological glucose level is thus important to ensure effective treatment.[22,23] In this context, fast and reliable detection of glucose has become very important in clinical diagnostics and biotechnological fields.[24] The existing method relies on the electrochemical oxidation of glucose by enzymes for detection in blood or serum samples because of their excellent selectivity, reliability, and good sensitivity.[25,26] However, the complex design of electrodes and the stability of the enzymes in the aggressive environment limit their full-scale exploitation. Moreover, the response of the enzymatic sensor is influenced by humidity, during use or storage; the presence of high or low humidity may have a detrimental effect on the sensor. Thus, it is important to develop a sensing tool that detects accurately the level of glucose both in vivo and in vitro.[27] In this context, economical electrooxidation catalysts with relatively simple preparation method, high sensitivity, fast response, good stability, and reproducibility have been thoroughly investigated.[22] Metal- or metal oxide-based nanostructures in sensor application are gaining wide popularity due to their high reactivity at the surface, catalytic efficiency, fast electron communications, and retention of the catalytic property for a long period of time.[22,27] Thus, the problems associated with biosensors (ie, enzymatic sensors), such as sensitivity, response time, and stability, can be overcome by employing suitable nanomaterials. Moreover, these nanostructures can significantly reduce the sensor size, thus reducing the cost factor; in addition, they can be used in continuous monitoring of urine, blood, or serum samples. Recently, CuO nanostructures have been investigated for biosensing applications because of their enhanced catalytic effect and resistance to surface poisoning.[28] CuO nanoparticles,[29] nanoplatelets,[30] nanowires,[27] nanoflowers, and nanorods[10] have been applied for glucose detection with good sensitivity. Most of the synthetic protocols for the formation of these attractive nanostructures are tedious and expensive. In contrast, a solution-phase synthesis of such structures is versatile and is suitable to fabricate a wide range of nanostructures with controlled sizes.

In this study, we employ a facile approach to synthesize spherulitic Cu–CuO nanostructures in toluene-in-water microemulsion using CTAB as the surfactant. The effect of the surfactant concentration on the morphological hierarchy of the resultant structures was also investigated. The Cu–CuO nanostructures were then deposited on a multiwalled carbon nanotube (MWCNT)-modified indium tin oxide (ITO) glass to obtain a composite electrode. The fabricated electrodes were applied for glucose oxidation in alkaline medium. The electrodes demonstrated good catalytic property for glucose oxidation vouching for the fabrication of a nonenzymatic glucose sensor.

Experimental

Materials

Copper acetate, CTAB, and sodium borohydride were purchased from Aldrich (Gyeonggi-do, South Korea). MWCNTs (>95 wt% purity, 10–15 nm in diameter) were purchased from Carbon Nano-material Technology Co., Ltd (Gyeongsangbuk-do, South Korea). It was used in the present investigation without further purification. All other chemicals used were of reagent grade.

Methods

The spherulitic Cu–CuO nanostructures were prepared by a modified protocol as developed by Song et al.[21] Toluene and water were used as the medium here. Typically, 10 mL of a 20 mM solution of copper acetate aged for 1 day was mixed

with 10 mL of a 30–50 mM solution of CTAB in toluene under stirring conditions. The solution was then transferred to a 250 mL glass beaker, and 80 mL of distilled water was added followed by 10 mL of $NaBH_4$ solution. The resulting mixture was stirred for 20 minutes at room temperature. The solution was then placed in an air oven and aged at 65°C for 3 days. Upon aging, the color of the solution changes from yellow to brownish, indicating the formation of CuO. The product obtained was treated with deionized water, and repeatedly centrifuged and washed with water and ethanol. Finally, the product was dried in a vacuum oven at 45°C overnight.

ITO glass (<20 ohm/sq) procured from Aldrich (Gyeonggi do, Korea) was used as the base electrode. The ITO glass was cut into dimension of 5 mm (width) and 20 mm (length). The working area of the ITO glass for the electrochemical tests was controlled to 0.25 cm^2.

Fabrication of the electrodes

The electrodes were prepared as follows. MWCNT dispersed in dimethylformamide (DMF) (1 mg/mL in DMF) was dropped onto the ITO electrode to get a uniform film. Afterward, 20 µL of Cu–CuO nanostructures (5 mg/mL in DMF) was dripped on the MWCNT-modified ITO glass. Finally, the electrodes were dried in a vacuum oven at 45°C overnight. The electrodes were denoted as ITO/MWCNT/Cu–CuO_X, where X=A, B, and C; A, B, and C designate the Cu–CuO nanostructure prepared in the presence of 30 mM, 40 mM, and 50 mM of CTAB, respectively.

Instruments

A JEOL JSM-6700F (Tokyo, Japan) scanning electron microscope was employed for the observation of the sample morphologies. The structures of the samples were observed using a high-resolution transmission electron microscope (JEOL JEM-4010, Tokyo, Japan) equipped with an energy-dispersive spectral analyzer. Prior to analysis, the powdered samples were dispersed in absolute ethanol by ultrasonication for 10 minutes in a KQ-250B ultrasonic bath. The samples were then placed on a copper grid; the sample-coated grid was dried in a vacuum oven. The X-ray diffraction (XRD) measurements of the samples were carried out with a Rigaku X-ray diffractometer with Cu Kα radiation (λ=1.5418 Å) at an operating voltage of 40 keV and 20 mA and a scan rate of 2°/min. The binding energy plots of the samples were obtained with an X-ray photoelectron spectrophotometer (K-alpha, Thermo VG, Cambridge, UK) using a monochromated Al X-ray source (Al Kα line: 1,486.6 eV).

Electrochemical measurements

The electrocatalytic activity of ITO/MWCNT/Cu–CuO electrodes was evaluated by cyclic voltammetry (CV) using a potentiostat–galvanostat (VSP, BioLogic-Science Instruments, 38640 CLAIX, France). A conventional three-electrode cell assembly was employed for the electrochemical measurements. ITO/MWCNT/Cu–CuO was used as the working electrode; Ag/AgCl and platinum wire were used as reference and counter electrodes, respectively. The CVs were obtained in aqueous NaOH (0.1 M) at room temperature under ambient conditions at a scan rate of 20 mV s^{-1}. All the measurements were performed at room temperature.

The chronoamperometric (CA) measurements of ITO/MWCNT/Cu–CuO_A, ITO/MWCNT/Cu–CuO_B, and ITO/MWCNT/Cu–CuO_C were carried out by adding aliquots of glucose solutions at regular intervals, and recording the corresponding current changes. A small magnetic bar provided the convective transport. The onset oxidation potential was taken as the detection potential in each case.

Results and discussion

Morphology and growth mechanism

The scanning electron microscopy (SEM) images of the nanostructures at low and high magnifications are shown in Figure 1. These images indicate that almost all structures show spherulitic growth. As can be visualized from the SEM micrographs, the structures are composed of a central core with clearly thin nanorod and nanowire outgrowths that radiate from the core to all directions, giving the structure a blooming appearance. The core of the nanostructures has a diameter of 100–150 nm, whereas the radial outgrowths were several nanometers long and 15–50 nm in diameter. Careful observation of the nano-architecture revealed that the outgrowths remained attached to the central core after prolonged time, suggesting that they were integrated in the structure and not just mere aggregations. A proposed mechanism is shown in Figure 2. The formation of reverse micelles by CTAB in oil-in-water systems has been well-documented in the literature.[15,16] However, there are no reports on the growth of such spherulitic structures by reverse micelle method. The high resistance of the toluene-in-water microemulsion is in agreement with previous findings for spherical inverse micelle formation.[21] In these vesicles, the metal ion preferentially resides in the interior pool of water, forming Cu^{2+}–Ac^- interactions with the ionic head group of CTAB. After, the addition of the reducing agent, there is a reduction of Cu^{2+} in the interior, and the individual particles may coalesce to form larger spherical

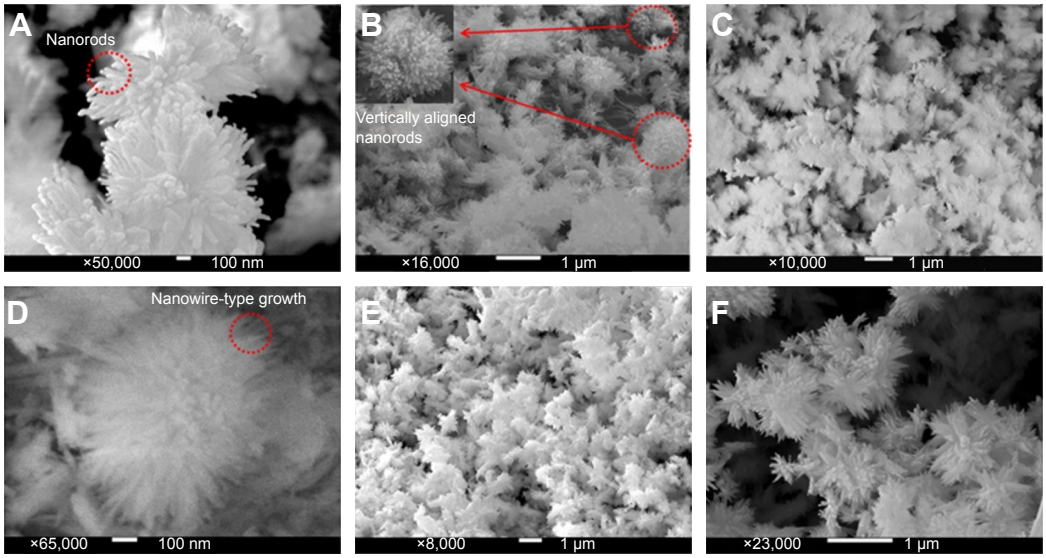

Figure 1 Morphological analysis.
Notes: SEM micrographs of (**A** and **B**) Cu–CuO_A. The dotted circles showed the enlarged view of vertically aligned nanorods in inset of Figure 1B. (**C** and **D**) Cu–CuO_B, and (**E** and **F**) Cu–CuO_C at low and high magnifications.
Abbreviation: SEM, scanning electron microscopy.

particles. These particles then serve as the seeds or nuclei from which the outgrowths merge.

A parallel experiment, in which the reaction was carried out in the absence of CTAB, was performed. However, in this case, only particle agglomerates were observed (Figure S1). Thus, it was found that the surfactant was required for the formation of the spherulitic-like morphology. The reduction of the copper salt proceeds slowly toward the end of

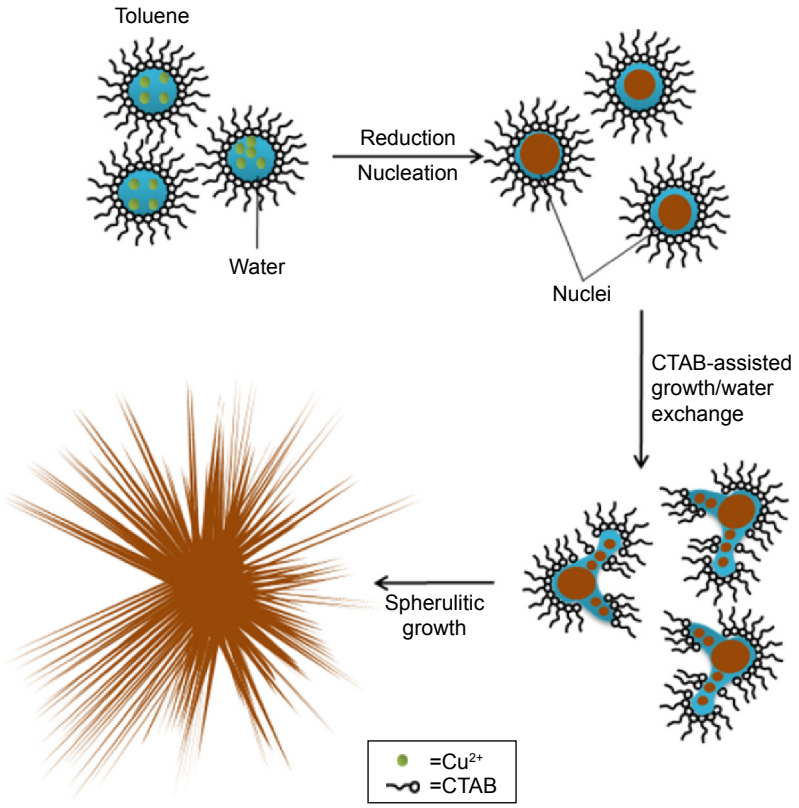

Figure 2 Schematic representation of the possible growth mechanism of the nanostructures.
Abbreviation: CTAB, cetyltrimethyl ammonium bromide.

the reaction; consequently, the resultant nanoparticles were forced to grow on the surface of the conglomerate. It has been previously reported that the presence of metal cations influences the interfacial tension at the oil/water interface.[31] Therefore, the local environment at the interface changes resulting in the different arrangements of the surfactant in the oil (toluene) phase. This might prompt CTAB to adopt a tubular arrangement at the interface, which guides the direct attachment of nanoparticles to the initially formed nuclei.

It has been established that CTAB acts as a structure-directing agent by preferentially adsorbing onto the metal facets.[32,33] This feature contributes to the assembly of the nanoparticles along a one-dimensional direction, resulting in the growth of nanorods/nanowires. Figure 1 shows the SEM images of the copper nanostructures using 30 mM, 40 mM, and 50 mM solutions of CTAB (Cu–CuO_A, Cu–CuO_B, and Cu–CuO_C, respectively). Spherulitic structures with uniform size of several hundred nanometers are observed. During aging, some of the urchin-like spherulites coalesced to form bigger structures. The concentration of CTAB was found to influence the spherulitic growth. The lowest thickness of the outgrowth was observed for Cu–CuO_B (Figure 1B and C); a possible explanation is that, at this concentration, the growth rate is minimized by the adsorption of the surfactant on the crystal surfaces, and at the same time, spatial repulsion among surfactant molecules would reduce the thickness of the outgrowths. The increased thickness of the outgrowth for Cu–CuO_C can be related to the constantly varying supersaturations contributing to the convoluted growth modes.

The spherulitic nanostructure of Cu–CuO was also observed by high-resolution transmission electron microscope. Figure 3 shows that radially arrayed outgrowths of 15–20 nm in diameter originate from the central core. The spherulitic structures are porous with large surface areas. Figure 3D reveals the polycrystalline nature of the nanostructures as the lattice fringe patterns have different orientations. The interplanar spacings were measured to be 0.17 nm and 0.23 nm, which correspond to Cu (111) and CuO (200), respectively.[34]

Optical and structural properties

The ultraviolet–visible (UV–vis) spectra of the CuO nanoparticles are illustrated in Figure 4A. The optical properties of CuO spherulitic-type structures show interesting features. The Cu–CuO_A and Cu–CuO_B structures showed a broad surface plasmon resonance (SPR) absorption band with maximum peak intensity centered at 441 nm and 433 nm, respectively. The wide absorption band results from the formation of a large number of highly dense nanoparticles on the surface of the nanostructures.[35] The characteristic absorption peak is due to plasma resonance excitation of the copper atoms on the surface of the nanostructures.[34,36] However, in case of Cu–CuO_C, the SPR band is observed at 370 nm, owing to the shape and distribution of particles in the nanostructures.[37] Additionally, for Cu–CuO_A, Cu–CuO_B, and Cu–CuO_C, small bands at 237 nm, 233 nm, and 235 nm are observed in the UV–vis spectra. These bands correspond to the interband transition of the core electrons of copper metal. The band gaps of copper oxide nanostructures were calculated at 441 nm, 433 nm, and 370 nm for the Cu–CuO nanostructures from UV–vis spectra, by using the following equation.[38]

$$\alpha = \frac{C(h\nu - E_g)\eta}{h\nu} \quad (1)$$

where α is the absorption coefficient, C is a constant, $h\nu$ is the photon energy, and E_g is the bulk band gap. Power η is a constant whose value for copper oxide-based materials is 1/2, which corresponds to the directly allowed transition.[39] The band gaps were obtained by extrapolating the intercept of the fitted line with the $h\nu$ axis (Figure 4B). The band gaps for Cu–CuO_A, Cu–CuO_B, and Cu–CuO_C were found to be 1.28 eV, 1.36 eV, and 1.42 eV, respectively, which is in agreement with previously reported values.[40] This increase in the band energy gap of the CuO nanostructures is indicative of quantum size effects.[40]

Figure 4C shows the XRD pattern of the copper–copper oxide nanoparticles synthesized by the soft template approach. The XRD diffractogram shows distinct peaks for CuO at 32.3° (110), 35.2° (–111), 38.5° (111), 48.5° (–202), 53.2° (020), 57.8° (202), 61.4° (–113), 65.7° (–311), 67.5° (113), 72.1° (331), and 75.4° (004). The peaks can be indexed to a monoclinic phase of CuO (JCPDS 45-0937). Besides, the peaks at 43.3° evidenced the presence of Cu in the nanostructures. The binding energy plot of the nanostructures further confirms the formation of copper oxide structures (Figure S2).

Electrochemical measurements

The electrochemical activity of the Cu–CuO samples in alkaline medium is depicted in the CV plots shown in Figure 5. The electrodes exhibited no peaks in the measured potential range; however, upon addition of glucose, a sharp increase in the current is observed for the experimental Cu–CuO electrodes. However, the control electrode, that is, ITO/MWCNT, showed no variation in the current signal, indicating that

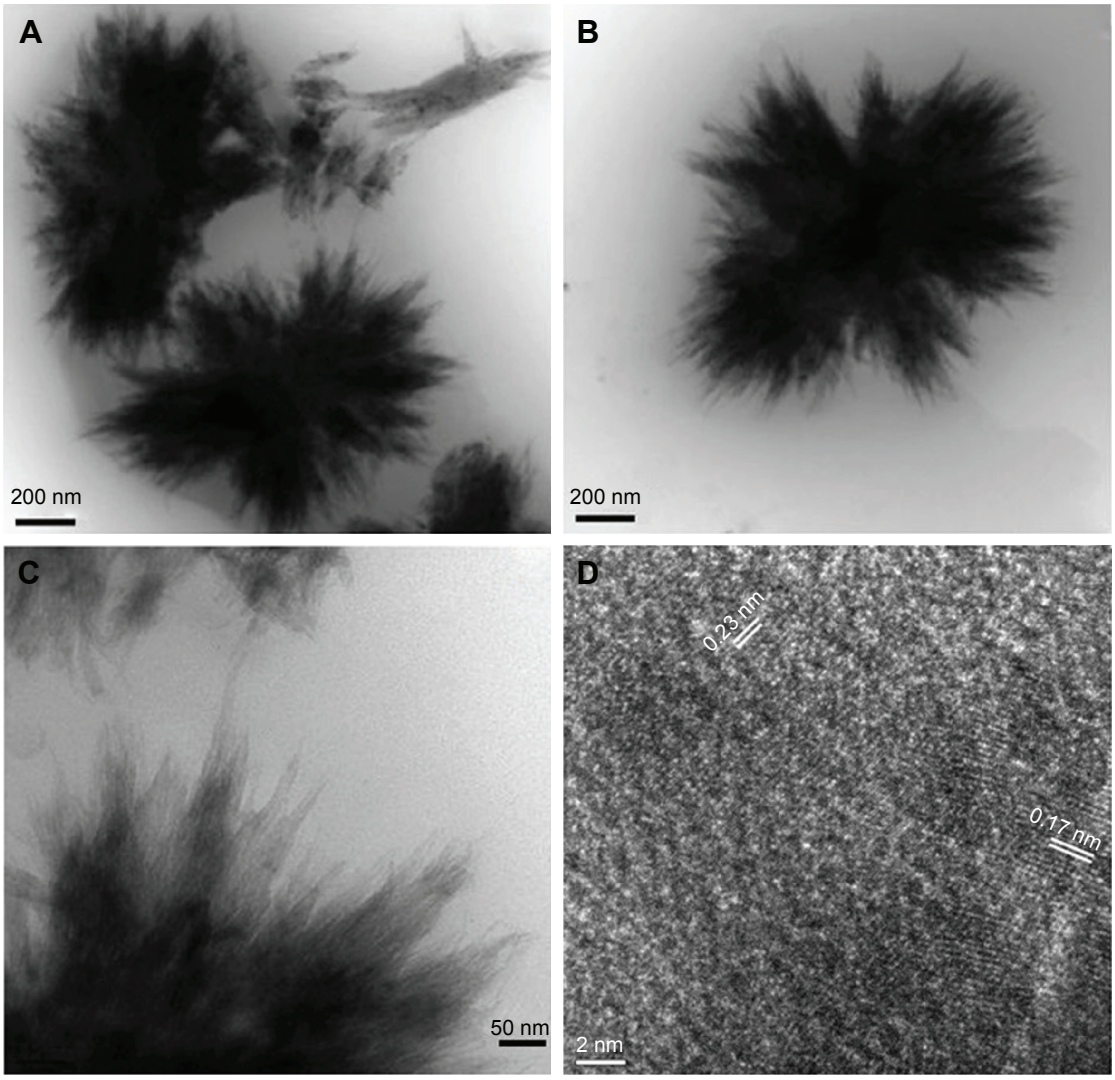

Figure 3 Transmission electron microscopy micrographs.
Notes: (**A**–**C**) Cu–CuO_B. (**D**) Lattice fringe pattern of Cu–CuO.

Cu–CuO was solely responsible for the catalytic oxidation of glucose. The morphology of the nanostructures played a significant role in tuning the electrochemical activity. ITO/MWCNT/Cu–CuO_B (Figure 6B) exhibited the highest current density of 4.19 mA cm^{-2} (after background current correction) at +0.9 V. Although no oxidation peak was detected in the plots, the current showed a sharp increase at potentials corresponding to the onset oxidation potential for glucose oxidation, which has been reported elsewhere.[10,41] The onset oxidation potential for ITO/MWCNT/Cu–CuO_A, ITO/MWCNT/Cu–CuO_B, and ITO/MWCNT/Cu–CuO_C was observed at +0.36 V, +0.34 V, and +0.15 V, respectively. The electrooxidation of glucose over copper-based material has been widely reviewed in the recent literature, and the formation of the redox couple Cu (II)–Cu (III) in an alkaline medium has been considered to play a significant role in the oxidation process.[41,42] The deprotonation of glucose and isomerization to the enediol form has been suggested to initiate the oxidation process.[43]

CA responses

CA studies were carried out in order to ascertain the performance of ITO/MWCNT/Cu–CuO_A, ITO/MWCNT/Cu–CuO_B, and ITO/MWCNT/Cu–CuO_C electrodes (Figure 6). The CA measurement was performed by the successive addition of aliquots of glucose solution under continuous stirring. In all cases, the current response reached 95% of steady state within 3–12 seconds (Figure S3), depending on the type of electrode. The ITO/MWCNT/Cu–CuO_B electrode showed the fastest response (3 sec-

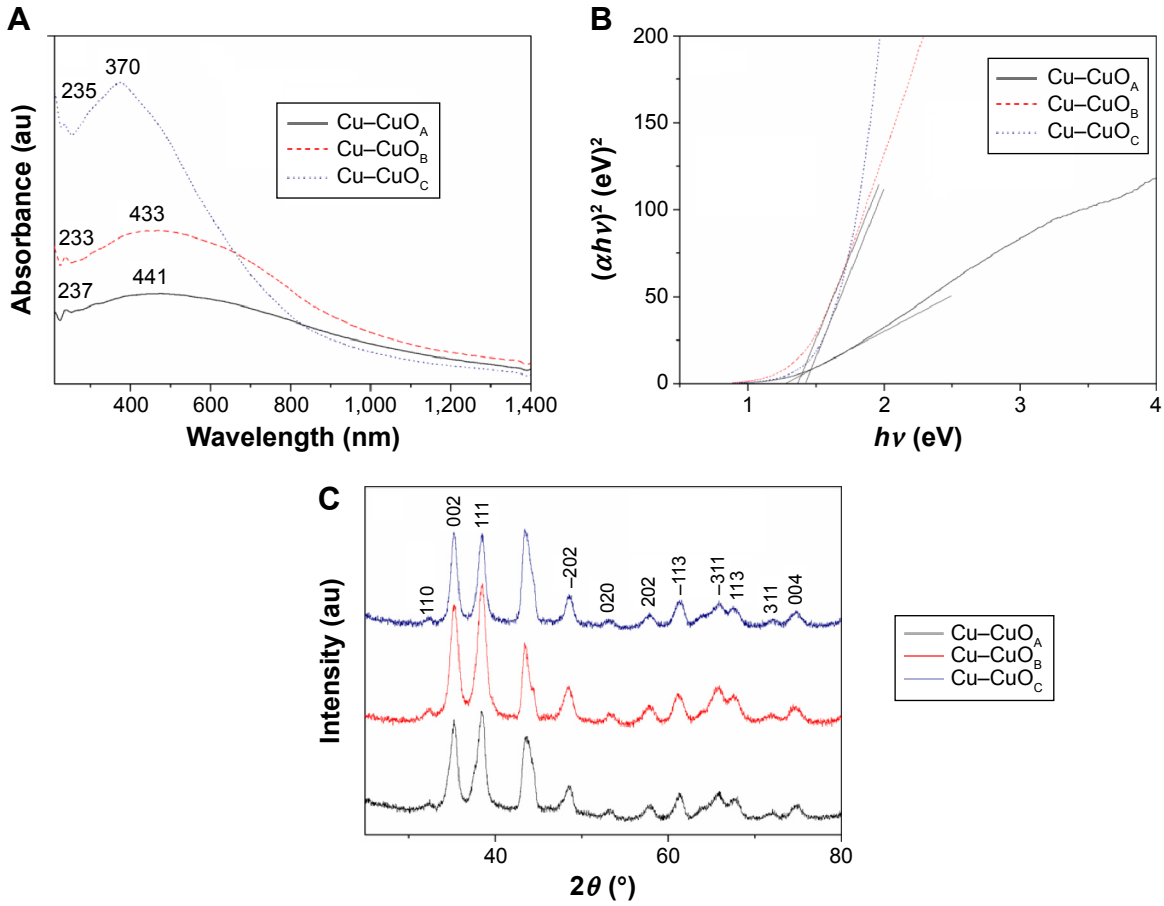

Figure 4 Optical and structural characteristics of Cu–CuO.
Notes: (**A**) UV–vis spectra. (**B**) Plot of $(\alpha h\nu)^2$ vs $h\nu$. (**C**) XRD diffractogram of Cu–CuO.
Abbreviations: UV–vis, ultraviolet–visible; XRD, X-ray diffractogram.

onds). The linear range was found to be 0.023–0.29 mM, 0.07–0.08 mM, and 0.023–0.34 mM for ITO/MWCNT/Cu–CuO$_A$, ITO/MWCNT/Cu–CuO$_B$, and ITO/MWCNT/Cu–CuO$_C$ with a correlation coefficient (R^2) of 0.989, 0.997, and 0.998, respectively. On further increasing the glucose concentration, the current plateaus at higher concentrations, indicating the saturation of the active sites of the Cu–CuO nanostructures. The sensor was calibrated by measuring the response three times, and the average value was plotted against the concentration. The ITO/MWCNT/Cu–CuO$_A$, ITO/MWCNT/Cu–CuO$_B$, and ITO/MWCNT/Cu–CuO$_C$ electrodes showed a very high sensitivity of 1,229, 3,012, and 3,642 μA mM^{-1}·cm^{-2}, respectively, in the linear range (Figure 6). As depicted in Table 1, the sensitivity of the ITO/MWCNT/Cu–CuO electrodes is higher than those reported for similar electrodes. The higher sensitivity results from the high density of the active surface area, which provides a better platform for an enhanced charge transfer behavior.[44] A detection limit of 2 μM was obtained for ITO/MWCNT/Cu–CuO$_B$ (Figure S3), which is comparable to reported values (Table 1). As shown in Table 1, the ITO/MWCNT/Cu–CuO$_B$ sensor exhibits better performance in terms of response time, sensitivity, and detection potential as compared with other nonenzymatic glucose sensors based on Cu–CuO structures.

Electrochemical analysis of MWCNT/Cu–CuO$_B$ electrode

The aforementioned observations show that ITO/MWCNT/Cu–CuO$_B$ exhibited the best performance; thus, this electrode was employed in the following investigation. The electrocatalytic activity of the ITO/MWCNT/Cu–CuO$_B$ electrode toward glucose oxidation was determined by CV measurements. Figure 7 depicts the CV in the absence and presence of glucose in the potential window of −0.2 V to +0.9 V. As stated earlier, no redox peaks were observed in the measured potential range, and a sharp increase in the current at +0.34 V was observed upon addition of glucose. Similar observations

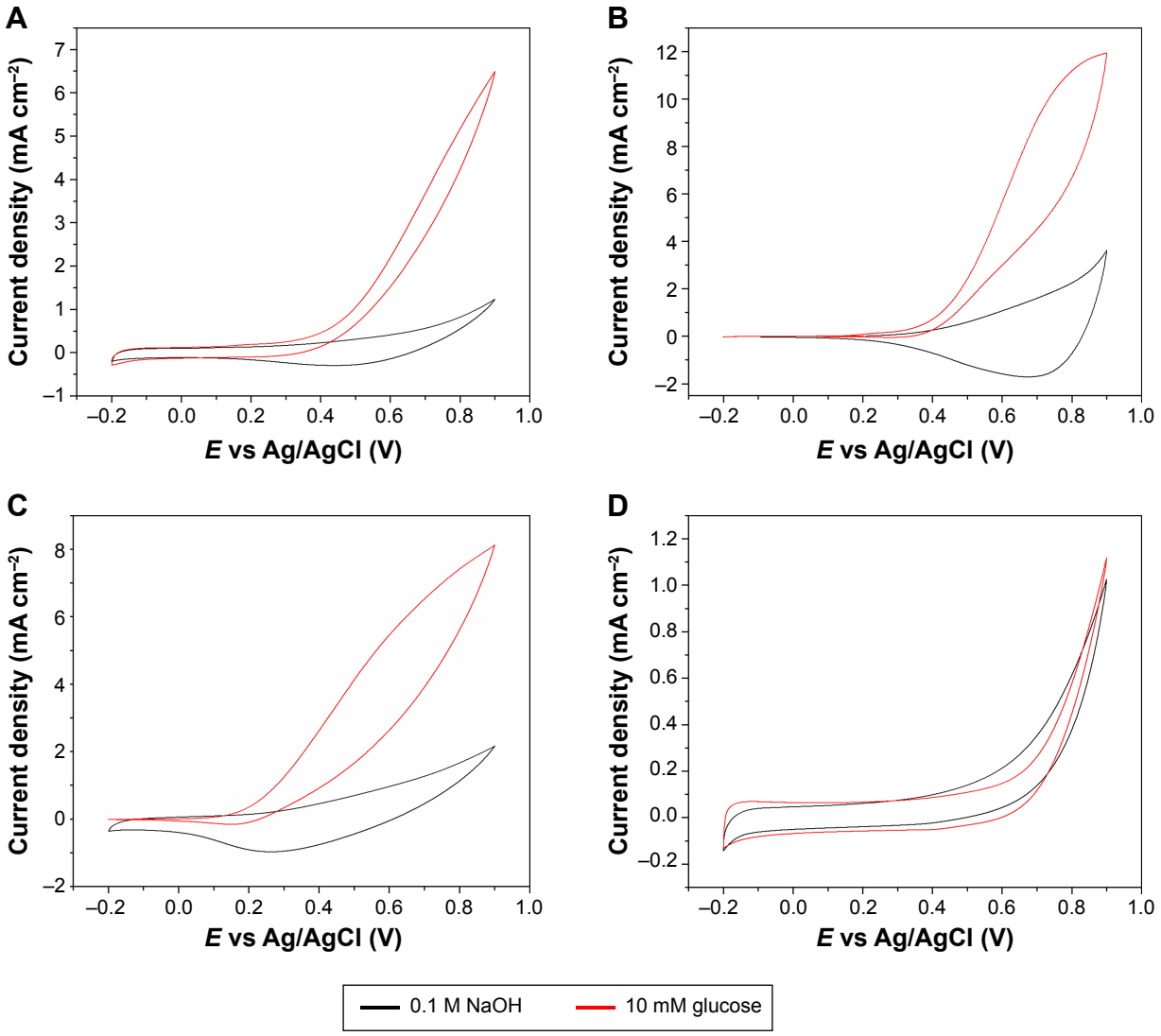

Figure 5 Electrochemical response plots of the different Cu-CuO electrodes.
Notes: Cyclic voltammograms obtained at 20 mV s^{-1} for (**A**) ITO/MWCNT/Cu–CuO_A, (**B**) ITO/MWCNT/Cu–CuO_B, (**C**) ITO/MWCNT/Cu–CuO_C, and (**D**) ITO/MWCNT, in the absence and in the presence of a 10 mM glucose solution.
Abbreviations: ITO, indium tin oxide; MWCNT, multiwalled carbon nanotube.

were made for CuO nanoparticles,[45] and CuO nanowires grown on the Cu surface.[46] The dramatic enhancement in the current toward the positive potential end for ITO/MWCNT/Cu–CuO_B indicates a remarkable increase in the catalytic activity. The presence of nanoscale wire and rod outgrowths generates a high surface-to-volume ratio and a large surface area. Moreover, the higher electronic conductivity of MWCNT accelerates the electron transfer rate enhancing the performance of the electrodes.

The variation of the current densities at different pH values is shown in Figure 8. A nonlinear variation of the current at the concentration range of NaOH from 0.01 M to 0.1 M was observed. The sharp increase in the current is due to the ease of glucose oxidation at elevated pH values. However, on increasing the concentration beyond 0.1 M, the current decreases and shows leveling off at higher values, presumably because of the blocking effect of excess OH^- on the deposition of glucose anion on the electrode.[47]

Interference, anti-poisoning property, and real-sample analysis

In order to assess the selectivity and response of the ITO/MWCNT/Cu–CuO_B electrode, the electrocatalytic properties were examined in the presence of common interfering species such as urea, cystamine, L-ascorbic acid, and creatinine. The CA response of the electrode was recorded by successively adding 0.1 mM of glucose and the interfering species at a detection potential of +0.34 V. As observed in Figure 9A,

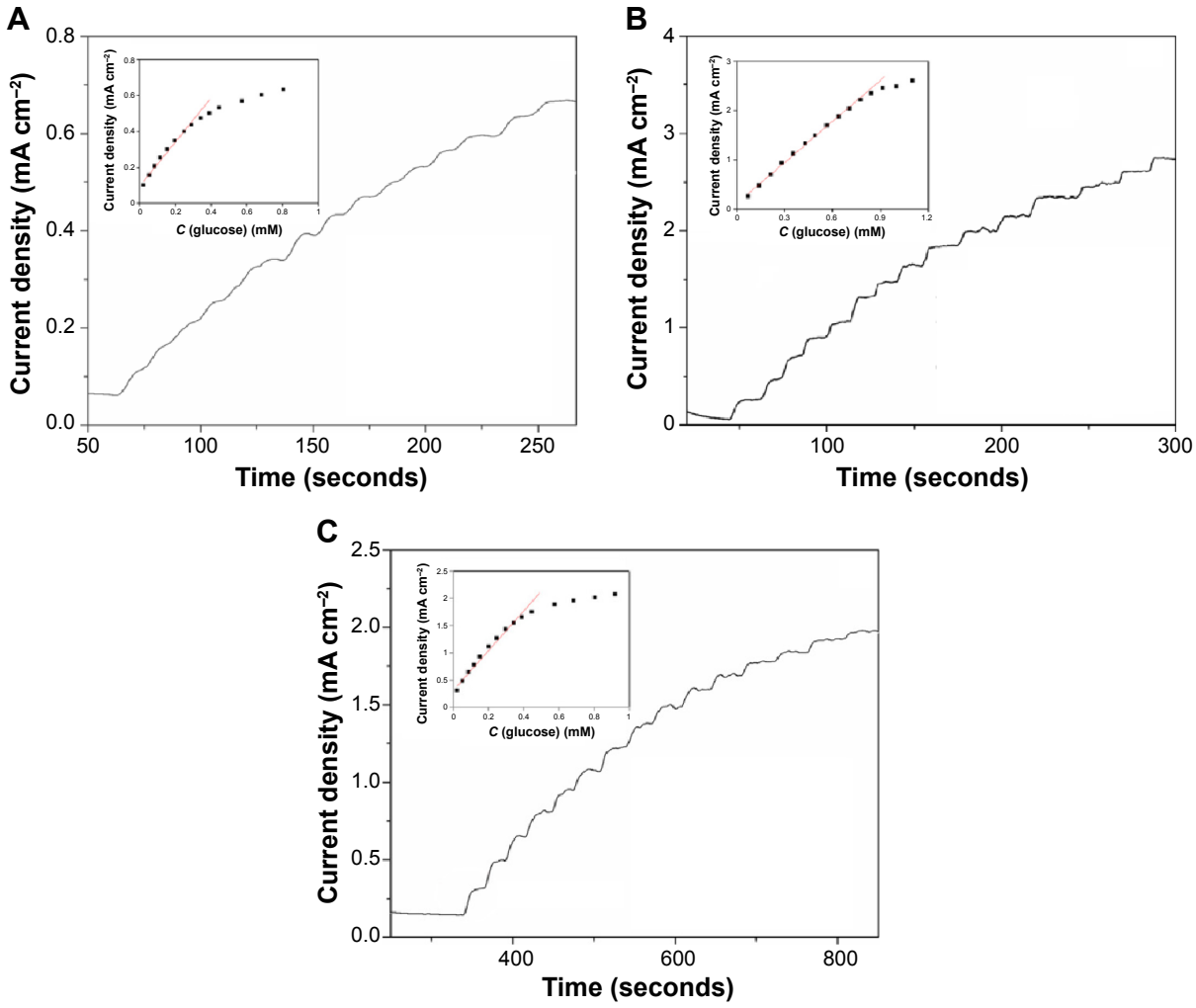

Figure 6 Current vs time curves.
Notes: Chronoamperometric curve of (**A**) MWCNT/Cu–CuO_A, (**B**) MWCNT/Cu–CuO_B, and (**C**) MWCNT/Cu–CuO_C measured at an applied potential of +0.36 V, +0.34 V, and +0.15 V with the successive addition of glucose solution. Inset: linear calibration curves of current vs glucose concentration.
Abbreviation: MWCNT, multiwalled carbon nanotube.

Table 1 Performances of some of the reported copper-based glucose sensors

Electrode	Linear range (mM)	Detection limit (mM)	Sensitivity ($\mu A\ mM^{-1}\cdot cm^{-2}$)	Response time (s)	Detection potential (V)	References
CuO NF/GCE	0.006–2.5	0.00080	431.3	1	–	25
CuO flower-like nanostructures/GOx	0.01–10	0.0013	47.19	<5	+0.58	48
Cu–CuO NW	0.1–12	0.05	17.7	5	+0.30	49
CuO flowers/G	–	0.004	709.52	>15	+0.60	50
CuO NS	0.05–2.5	0.001	404.53	–	+0.60	42
CuO/G	0.002–0.2	0.0002	–	3	+0.55	45
Cu nanocluster/MWCNT/GCE	0.0007–3.5	0.00021	17.76	5	+0.65	51
CuO–MWCNT/TA foil	0.0004–1.2	0.00020	2,596	1	–	30
Nafion/Cu–N-G/GCE	0.004–4.5	0.0013	48.13	<5	+0.50	52
NPG/CuO	Up to 12	0.0028	374.0	>10	+0.40	53
MWCNT/Cu–CuO_A	0.023–0.29	0.015	1,229.20	9	+0.36	Current work
MWCNT/Cu–CuO_B	0.07–0.8	0.002	3,012.10	~3	+0.34	Current work
MWCNT/Cu–CuO_C	0.023–0.34	0.005	3,642.70	~13	+0.15	Current work

Abbreviations: NF, nanofiber; GCE, glassy carbon electrode; GOx, glucose oxidase; NW, nanowire; G, graphene; NS, nanosphere; MWCNT, multiwalled carbon nanotube; TA, titanium aluminum; N-G, nitrogen-doped graphene; NPG, nanoporous gold; s, seconds.

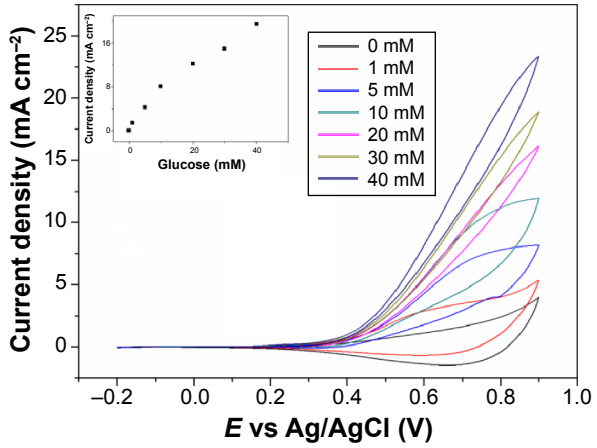

Figure 7 Cyclic voltammogram obtained at 20 mV s^{-1} for ITO/CNT/Cu–CuO_B at different glucose concentrations in 0.1 M NaOH.
Abbreviations: ITO, indium tin oxide; CNT, carbon nanotube.

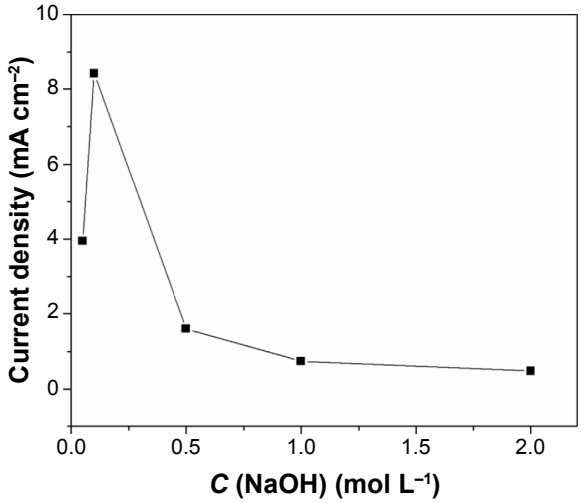

Figure 8 Effect of NaOH concentration on the current density (at +0.9 V) measured for ITO/MWCNT/Cu–CuO_B electrode in a 10 mM glucose solution.
Abbreviations: ITO, indium tin oxide; MWCNT, multiwalled carbon nanotube.

the ITO/MWCNT/Cu–CuO_B electrode showed a negligible response to the foreign species, indicating the electrode's high selectivity for glucose. Moreover, chloride poisoning of the electrode was analyzed from the CV of ITO/MWCNT/Cu–CuO_B in the presence and absence of 1 mM NaCl in 0.1 M NaOH. In both cases, the CV curves (Figure 9B) showed no significant variation, suggesting that ITO/MWCNT/Cu–CuO_B was resistant to chloride poisoning.

The feasibility of the ITO/MWCNT/Cu–CuO_B electrode to detect glucose in real urine and blood samples was evaluated by measuring the current response of diluted urine and blood collected from a normal person in a ratio of 1:100 in 0.1 M NaOH solutions. The diluted urine and blood was spiked with a known concentration of glucose solution, and the electrode response was recorded; for comparison, current was also recorded for the same concentrations of glucose solutions in 0.1 M NaOH without the real samples. Table 2 summarizes the glucose estimation in the real samples. The experimental results exhibited that the ITO/MWCNT/Cu–CuO_B electrode is feasible as a glucose sensor.

Conclusion

The present study demonstrates the formation of hierarchical superstructures by a simple wet chemical approach under ambient conditions. The obtained Cu–CuO structures showed high electrocatalytic activity for glucose oxidation. A high sensitivity (3,012 µA $mM^{-1}·cm^{-2}$) and a fast response time (3 seconds) were observed for the ITO/MWCNT/Cu–CuO_B electrode. Thus, the Cu–CuO-based nanomaterial exhibits

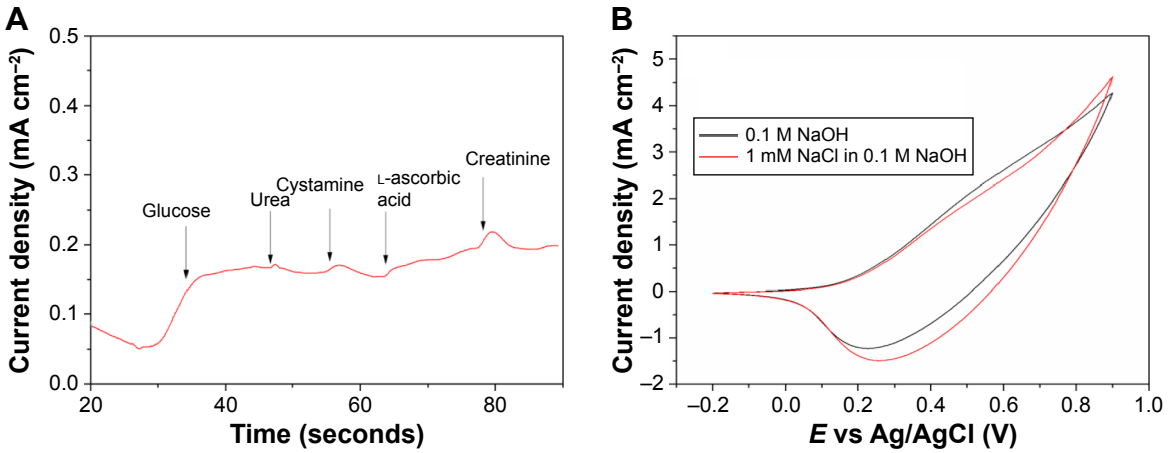

Figure 9 Specificity and stability test curves.
Notes: (**A**) Interfering response and (**B**) poisoning effect of MWCNT/Cu–CuO_B electrode.
Abbreviation: MWCNT, multiwalled carbon nanotube.

Table 2 Estimation report of glucose in urine and blood

Glucose added (mM)	Glucose recovered (mM)	Recovery (%)
Urine		
0.01	0.013	135
0.03	0.024	80
0.05	0.040	80
0.07	0.049	70
Blood		
0.01	0.012	81
0.03	0.028	106
0.05	0.031	160
0.07	0.062	111

potential to be utilized in the fabrication of high-performance and cost-effective microscale sensor devices.

Acknowledgment

This work was supported by the Gyeonggi Regional Research Center.

Disclosure

The authors report no conflicts of interest in this work.

References

1. Xu L, Sithambaram S, Zhang Y, et al. Novel urchin-like CuO synthesized by a facile reflux method with efficient olefin epoxidation catalytic performance. *Chem Mater*. 2009;21(7):1253–1259.
2. Zhang T, Dong W, Keeter-Brewer M, Konar S, Njabon RN, Tian ZR. Site-specific nucleation and growth kinetics in hierarchical nanosyntheses of branched ZnO crystallites. *J Am Chem Soc*. 2006; 128(33):10960–10968.
3. Zhang Q, Zhang K, Xu D, et al. CuO nanostructures: synthesis, characterization, growth mechanisms, fundamental properties, and applications. *Prog Mater Sci*. 2014;60:208–337.
4. Das G, Kalita RD, Gogoi P, Buragohain AK, Karak N. Antibacterial activities of copper nanoparticle-decorated organically modified montmorillonite/epoxy nanocomposites. *Appl Clay Sci*. 2014;90:18–26.
5. Zhang J, Ma J, Shibo Z, Wenchang W, Chen Z. A highly sensitive nonenzymatic glucose sensor based on CuO nanoparticles decorated carbon spheres. *Sens Actuators B Chem*. 2015;211:385–391.
6. Akhavan O, Ghaderi E. Copper oxide nanoflakes as highly sensitive and fast response self-sterilizing biosensors. *J Mater Chem*. 2011; 21(34):12935–12940.
7. Akgul G, Akgul FA, Mulazimoglu E, Unalan HE, Turan R. Fabrication and characterization of copper oxide-silicon nanowire heterojunction photodiodes. *J Phys D Appl Phys*. 2014;47:0650106–0650113.
8. Morales J, Sanchez L, Martin F, Ramos-Barrado J, Sanchez M. Use of low-temperature nanostructured CuO thin films deposited by spray-pyrolysis in lithium cells. *Thin Solid Films*. 2005;474(1):133–140.
9. Li K, Fan G, Yang L, Li F. Novel ultrasensitive non-enzymatic glucose sensors based oncontrolled flower-like CuO hierarchical films. *Sens Actuators B Chem*. 2014;199:175–182.
10. Zoolfakar AS, Rani RA, Morfa AJ, O'Mullane AP, Zadeh KK. Nanostructured copper oxide semiconductors: a perspective on materials, synthesis methods and applications. *J Mater Chem C*. 2014;2:5247–5270.
11. Liu B, Zeng HC. Mesoscale organization of CuO nanoribbons: formation of "dandelions". *J Am Chem Soc*. 2004;126(26):8124–8125.
12. Jiang T, Wang Y, Meng D, Wu X, Wang J, Chen J. Controllable fabrication of CuO nanostructure by hydrothermal method and its properties. *Appl Surf Sci*. 2014;311:602–608.
13. Zhang YX, Huang M, Kuang M, et al. Facile synthesis of mesoporous CuO nanoribbons for electrochemical capacitors applications. *Int J Electrochem Sci*. 2013;8:1366–1381.
14. Keyson D, Volanti D, Cavalcante L, Simões AZ, Varela JA, Longo E. CuO urchin-nanostructures synthesized from a domestic hydrothermal microwave method. *Mater Res Bull*. 2008;43(3):771–775.
15. Eastoe J, Hollamby MJ, Hudson L. Recent advances in nanoparticle synthesis with reversed micelles. *Adv Colloid Interface Sci*. 2006; 128–130:5–15.
16. Lin X, Sorensen C, Klabunde K, Hadjipanayis G. Temperature dependence of morphology and magnetic properties of cobalt nanoparticles prepared by an inverse micelle technique. *Langmuir*. 1998; 14(25):7140–7146.
17. Ranjan R, Vaidya S, Thaplyal P, Qamar M, Ahmed J, Ganguli AK. Controlling the size, morphology, and aspect ratio of nanostructures using reverse micelles: a case study of copper oxalate monohydrate. *Langmuir*. 2009;25(11):6469–6475.
18. Zhou G, Lu M, Yang Z. Aqueous synthesis of copper nanocubes and bimetallic copper/palladium core-shell nanostructures. *Langmuir*. 2006; 22(13):5900–5903.
19. Ahmad T, Chopra R, Ramanujachary K, Lofland S, Ganguli A. Canted antiferromagnetism in copper oxide nanoparticles synthesized by the reverse-micellar route. *Solid State Sci*. 2005;7(7):891–895.
20. Dodoo-Arhin D, Leoni M, Scardi P, Garnier E, Mittiga A. Synthesis, characterisation and stability of Cu_2O nanoparticles produced via reverse micelles microemulsion. *Mater Chem Phys*. 2010;122(2):602–608.
21. Song Y, Garcia RM, Dorin RM, et al. Synthesis of platinum nanowire networks using a soft template. *Nano Lett*. 2007;7(12):3650–3655.
22. Taguchi M, Ptitsyn A, McLamore ES, Claussen JC. Nanomaterial-mediated biosensors for monitoring glucose. *J Diabetes Sci Technol*. 2014;8(2):403–411.
23. Veiseh O, Tang BC, Whitehead KA, Anderson DG, Langer R. Managing diabetes with nanomedicine: challenges and opportunities. *Nat Rev Drug Discov*. 2015;14:45–57.
24. Rakhi RB, Sethupathi K, Ramaprabhu S. A glucose biosensor based on deposition of glucose oxidase onto crystalline gold nanoparticle modified carbon nanotube electrode. *J Phys Chem B*. 2009; 113(10):3190–3194.
25. Lin Y, Lu F, Tu Y, Ren Z. Glucose biosensors based on carbon nanotube nanoelectrode ensembles. *Nano Lett*. 2004;4(2):191–195.
26. Halámková L, Halámek J, Bocharova V, Szczupak A, Alfonta L, Katz E. Implanted biofuel cell operating in a living snail. *J Am Chem Soc*. 2012; 134(11):5040–5043.
27. Wang W, Zhang L, Tong S, Li X, Song W. Three-dimensional network films of electrospun copper oxide nanofibers for glucose determination. *Biosens Bioelectron*. 2009;25(4):708–714.
28. Makaram P, Owens D, Aceros J. Trends in nanomaterial-based non-invasive diabetes sensing technologies. *Diagnostics*. 2014;4(2): 27–46.
29. Luo P, Zhang F, Baldwin RP. Comparison of metallic electrodes for constant-potential amperometric detection of carbohydrates, amino acids and related compounds in flow systems. *Anal Chim Acta*. 1991; 244(0):169–178.
30. Jiang L-C, Zhang W-D. A highly sensitive nonenzymatic glucose sensor based on CuO nanoparticles-modified carbon nanotube electrode. *Biosens Bioelectron*. 2010;25(6):1402–1407.
31. Wang J, Zhang W-D. Fabrication of CuO nanoplatelets for highly sensitive enzyme-free determination of glucose. *Electrochim Acta*. 2011;56(22):7510–7516.
32. Wojciechowski K, Bitner A, Warszyński P, Żubrowska M. The Hofmeister effect in zeta potentials of CTAB-stabilised toluene-in-water emulsions. *Colloids Surf A Physicochem Eng Asp*. 2011;376(1–3):122–126.
33. Sun X, Chen X, Deng Z, Li Y. A CTAB-assisted hydrothermal orientation growth of ZnO nanorods. *Mater Chem Phys*. 2003;78(1):99–104.

34. Zou Y, Li Y, Zhang N, Liu X. Flower-like CuO synthesized by CTAB-assisted hydrothermal method. *Bull Mater Sci*. 2011;34(4):967–971.
35. Teng F, Yao W, Zheng Y, et al. Synthesis of flower-like CuO nanostructures as a sensitive sensor for catalysis. *Sens Actuators B Chem*. 2008; 134(2):761–768.
36. Mandke MV, Han S-H, Pathan HM. Growth of silver dendritic nanostructures via electrochemical route. *Cryst Eng Comm*. 2011;14(1):86–89.
37. Gou L, Murphy CJ. Controlling the size of Cu_2O nanocubes from 200 to 25 nm. *J Mater Chem*. 2004;14(4):735–738.
38. Link S, El-Sayed MA. Shape and size dependence of radiative, non-radiative and photothermal properties of gold nanocrystals. *Int Rev Phys Chem*. 2000;19(3):409–453.
39. Thakur S, Karak N. Green reduction of graphene oxide by aqueous phytoextracts. *Carbon.* 2012;50(14):5331–5339.
40. Neskovska R, Ristova M, Velevska J, Ristov M. Electrochromism of the electroless deposited cuprous oxide films. *Thin Solid Films*. 2007; 515(11):4717–4721.
41. Akhavan O, Tohidi H, Moshfegh A. Synthesis and electrochromic study of sol-gel cuprous oxide nanoparticles accumulated on silica thin film. *Thin Solid Films*. 2009;517(24):6700–6706.
42. Li C, Su Y, Zhang S, Lv X, Xia H, Wang Y. An improved sensitivity nonenzymatic glucose biosensor based on a CuxO modified electrode. *Biosens Bioelectron*. 2010;26(2):903–907.
43. Reitz E, Jia W, Gentile M, Wang Y, Lei Y. CuO nanospheres based non-enzymatic glucose sensor. *Electroanalysis*. 2008;20(22):2482–2486.
44. Marioli JM, Kuwana T. Electrochemical characterization of carbohydrate oxidation at copper electrodes. *Electrochim Acta*. 1992; 37(7):1187–1197.
45. Zhang X, Wang G, Liu X, et al. Different CuO nanostructures: synthesis, characterization, and applications for glucose sensors. *J Phys Chem C*. 2008;112(43):16845–16849.
46. Yu H-Y, Xu M-Q, Yu S-H, Zhao G-C. A novel non-enzymatic glucose sensor based on CuO-graphene nanocomposites. *Int J Electrochem Sci*. 2013;8:8050–8057.
47. Zhuang Z, Su X, Yuan H, Sun Q, Xiao D, Choi MM. An improved sensitivity non-enzymatic glucose sensor based on a CuO nanowire modified Cu electrode. *Analyst*. 2008;133(1):126–132.
48. Wang YZ, Zhong H, Li XM, et al. Perovskite $LaTiO_3$-Ag0.2 nanomaterials for nonenzymatic glucose sensor with high performance. *Biosens Bioelectron*. 2013;48(0):56–60.
49. Umar A, Rahman M, Al-Hajry A, Hahn Y-B. Enzymatic glucose biosensor based on flower-shaped copper oxide nanostructures composed of thin nanosheets. *Electrochem Commun*. 2009;11(2):278–281.
50. Wang G, Wei Y, Zhang W, Zhang X, Fang B, Wang L. Enzyme-free amperometric sensing of glucose using Cu-CuO nanowire composites. *Microchimica Acta*. 2010;168(1–2):87–92.
51. Kang X, Mai Z, Zou X, Cai P, Mo J. A sensitive nonenzymatic glucose sensor in alkaline media with a copper nanocluster/multiwall carbon nanotube-modified glassy carbon electrode. *Anal Biochem*. 2007; 363(1):143–150.
52. Jiang D, Liu Q, Wang K, et al. Enhanced non-enzymatic glucose sensing based on copper nanoparticles decorated nitrogen-doped graphene. *Biosens Bioelectron*. 2014;54:273–278.
53. Xiao X, Wang M, Li H, Pan Y, Si P. Non-enzymatic glucose sensors based on controllable nanoporous gold/copper oxide nanohybrids. *Talanta*. 2014;125:366–371.

Supplementary materials

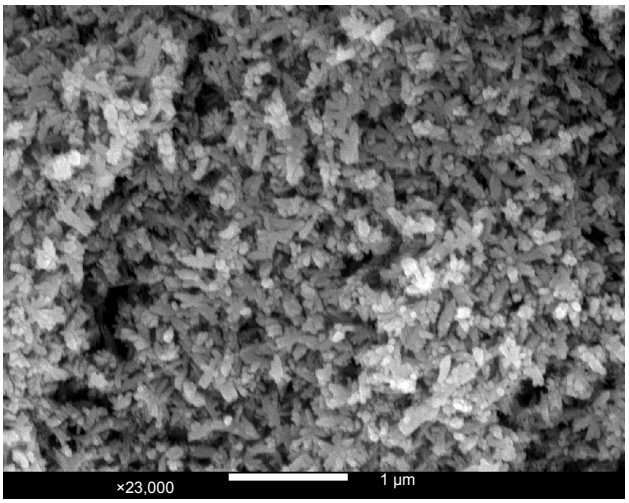

Figure S1 SEM micrograph of Cu–CuO_B obtained without the addition of CTAB in water-in-toluene system.
Note: In the absence of CTAB, particle agglomerates were predominantly formed.
Abbreviations: SEM, scanning electron microscopy; CTAB, cetyltrimethyl ammonium bromide.

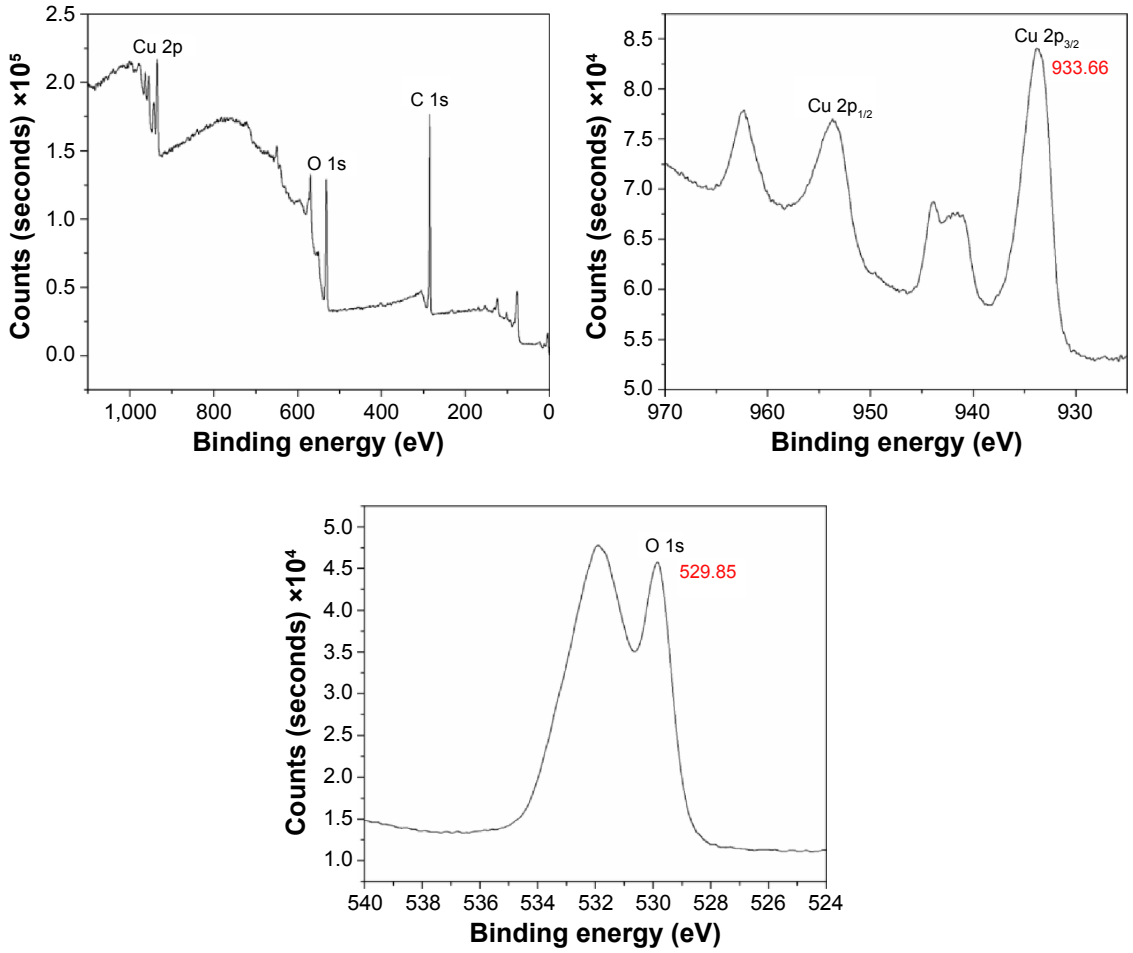

Figure S2 Binding energy plot of spherulitic Cu–CuO_B.
Notes: The XPS spectrum confirms the presence of Cu and O in the sample. The binding energies of Cu $2p_{3/2}$, and O 1s were observed at approximately 933.66 eV and 529.85 eV, respectively. The peaks of Cu $2p_{1/2}$ and Cu 2p indicate that Cu is in the +2 oxidation state.
Abbreviation: XPS, X-ray photoelectron spectrophotometry.

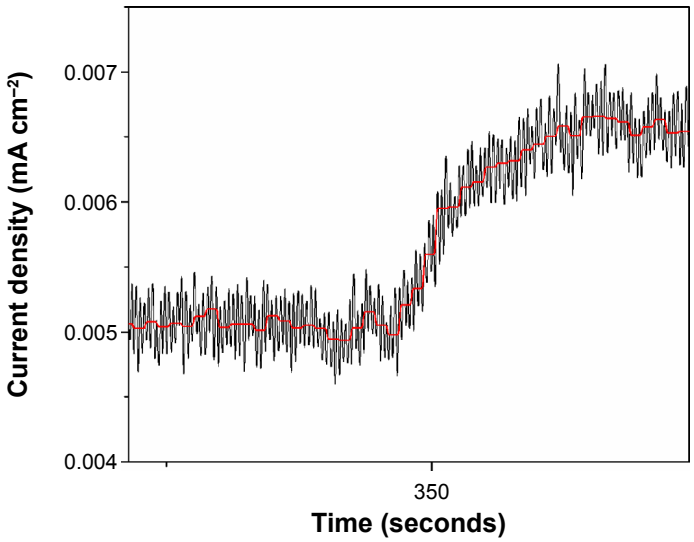

Figure S3 A typical amperometric response curve obtained for 2 μM glucose of the ITO/MWCNT/Cu–CuO_B electrode.
Abbreviations: ITO, indium tin oxide; MWCNT, multiwalled carbon nanotube.